crystals

Article

Experimental Study on the Thermal Conductivity of Improved Graphite Composite Insulation Boards

Genbao Liu [1], Yutao Guo [2], Zhiyu Jian [3], Mojia Huang [4] and Tengfei Zhao [3,*]

1. Design and Research Institute of Nanchang University, Nanchang University, 235 East Nanjing Road, Nanchang 330096, China
2. Institute for Ocean Engineering, Tsinghua Shenzhen International Graduate School, Shenzhen 518055, China
3. College of City Construction, Jiangxi Normal University, 99 Ziyang Avenue, Nanchang 330022, China
4. Institute of Engineering Mechanics, Nanchang University, 999 Xuefu Avenue, Nanchang 330031, China

* Correspondence: 005539@jxnu.edu.cn

Abstract: The thermal conductivity of thermal insulation materials directly affects the building energy consumption. The types and constituents of thermal insulation materials in thermal insulation boards are the key to determining the insulation performance. By optimizing the material constituents and ratios, this paper proposes an improved graphite composite insulation board (GCIB), which has lower thermal conductivity and good fire resistance. Through theoretical derivation, it is found that the limit range of the thermal conductivity of the new GCIB is 0.042–0.064 W/(m · K). Combined with the results of theoretical value analysis, and according to the ratios of material components, the random distribution function of each material component is constructed, and the numerical model of GCIB is established. Through numerical analysis, the range of thermal conductivity of the new composite insulation board is 0.046–0.050 W/(m · K). Finally, we establish an experimental model of the new GCIB. Through the model test of six GCIBs, the thermal conductivity of the new GCIB is obtained as 0.046 W/(m · K), which is in good agreement with the results of theoretical analysis and numerical simulation. Through theoretical analysis, numerical simulation and a sample test, this paper verifies the better thermal insulation performance of the improved GCIB, providing theoretical and numerical simulation methods for the new GCIB, as well as a theoretical reference for the promotion and application of the GCIB.

Keywords: thermal conductivity; graphite composite insulation board; thermal insulation performance; theoretical analysis; numerical simulation; sample test

Citation: Liu, G.; Guo, Y.; Jian, Z.; Huang, M.; Zhao, T. Experimental Study on the Thermal Conductivity of Improved Graphite Composite Insulation Boards. *Crystals* **2023**, *13*, 102. https://doi.org/10.3390/cryst13010102

Academic Editor: Tomasz Sadowski

Received: 27 November 2022
Revised: 31 December 2022
Accepted: 1 January 2023
Published: 5 January 2023

1. Introduction

In recent years, the global energy expenditure in industrial and residential construction has become one of the most important concerns [1]; due to industrial development and population growth, the amount of housing, industry, commerce and urban construction will increase significantly. It is estimated that the global energy consumption will increase by 64% by 2040 [2]. Therefore, in order to achieve the sustainable development of the country and society, it is necessary to use thermal insulation materials to better save energy and strengthen the sustainable energy strategy of the construction sector. The construction industry improves its energy efficiency by continuously developing new thermal insulation materials. The thermal insulation efficiency of thermal insulation materials mainly depends on the thermal conductivity and their ability to maintain their thermal characteristics for a period of time. Thermal conductivity is one of the main characteristics of thermal insulation materials in the building industry. The most accurate method to obtain the thermal conductivity of composite insulation board is to measure it according to the standard test method [3]. The thermal insulation of the building envelope is very important for energy conservation and a comfortable indoor environment. For the envelope of a building structure, the lower the thermal conductivity is, the better the thermal insulation performance of the materials is, and the higher the energy conservation rate of the building is. However, the thermal insulation materials are mostly flammable materials, and the improvement of the thermal insulation performance will reduce the fire resistance of the building structure. Therefore, on the premise of ensuring the fire protection requirements of building structure maintenance component materials, it is crucial to improve the thermal insulation performance of building structures by adjusting and improving the thermal conductivity of thermal insulation components in maintenance components.

As energy becomes increasingly scarce, thermal insulation materials are being forcibly used in buildings. Thermal insulation materials are a type of material or a combination of materials, usually composed of solid matrix materials and gas materials, and gas materials are randomly or regularly scattered in cells, pores or gaps [4,5]. Thermal insulation can be applied to certain structural components, including walls, roofs, ceilings, windows and floors [6]. Abu Jdayil et al. [7] reviewed the different types, manufacturing methods and characteristics of the traditional and most advanced thermal insulation materials in recent decades. Most of the available thermal insulation materials can be divided into four categories, including inorganic materials, organic materials, composite materials and advanced materials [8]. The consumption of inorganic materials accounts for 60% of the market, while that of organic insulating materials accounts for 27% [1]. According to the selection of thermal insulation materials for the exterior walls of public buildings in Jiangxi Province in 2019, the use of inorganic thermal insulation mortar accounted for 52.8%, rock wool board accounted for 28.0%, foamed cement accounted for 9.4%, inorganic nano silicon thermal insulation board accounted for 4.9%, vitrified micro bead board accounted for 4.6%, reflective thermal insulation coating for 0.1% and foam glass thermal insulation board for 0.2%, and most of the thermal insulation materials were inorganic materials. Lakatos et al. [9] used different methods to measure the thermal insulation performance of vacuum insulation board with an EPS protective layer, and they performed a comparative study. Berardi [10] studied the influence of environmental factors on the equivalent thermal conductivity of several foam materials. Kumar et al. [11] studied the performance of a variety of building insulation materials and gave a comparison of their performance in different climatic regions. Yang et al. [12] conducted research on the thermal conductivity of aerogel thermal insulation board for building energy conservation through numerical simulation and tests. König et al. [13] quantified the contribution of the effective thermal conductivity of open cell foam glass. Lamy-Mendes et al. [14] introduced the remarkable thermal conductivity of silica aerogel in the application of building thermal insulation. Li et al. [15] carried out a series of experimental studies on the thermal performance of vacuum insulation board and extruded polystyrene foam building walls. Wang et al. [16] studied the change in thermal conductivity of eight common building insulation materials (i.e., glass wool, rock wool, silicone blanket, foamed polystyrene, extruded polystyrene, phenolic foam, foam ceramics and foam glass) with temperature and relative humidity through experiments. Under different external conditions, many scholars have carried out a series of studies on the thermal conductivity of thermal insulation materials [6,7,17–19]. Petrosyan [20] studied the influence of the presence of thermal insulation in the structure on the cold load required for cooling, and revealed a pattern of cost changes in the case of insulating materials. Khoukhi [21] elucidated the combined impact of heat and humidity transfer on the thermal conductivity of polystyrene in building insulation materials. Berardi et al. [22] obtained the effects of accelerated aging processes in laboratory conditions over the thermal performance of aerogel-enhanced insulating materials. Berardi et al. [23] presented an experimental analysis of the thermal conductivity of four materials, namely rock wool, fiberglass, extruded polystyrene and polyisocyanurate, and explained how assumptions about thermal conductivity in simulations affect performance estimates. Al-Homoud [24] presented an overview of the performance characteristics and the main features of common building thermal insulating materials and their applications. Berardi et al. [25] took common insulating materials as examples (e.g., fiberglass, rock wool, polyisocyanurate and extruded polystyrene), and quantified the impact of the temperature dependency of the thermal conductivity in exterior walls and flat roofs. Wu et al. [26] investigated the thermal conductivity of polyurethane (PU) foams theoretically and experimentally. Hoseini et al. [27] presented a theoretical and experimental study on the effective thermal conductivity of aerogel composites. Majumder et al. [28] provided a detailed analysis for the thermal characterization of recycled materials for building insulation. While thermal insulation boards are mostly composed of a variety of materials, the ratios of thermal insulation materials will directly affect the thermal conductivity [1] and fire resistance [29] of thermal insulation boards. The ratios of each material component in building thermal insulation boards should comprehensively consider the thermal conductivity, fire resistance and other factors, which is relatively lacking in research. The GCIB uses highly flame-retardant graphite composite polystyrene particles as a filler, high-strength inorganic polymer materials as a binder and a proper amount of functional additives. It is processed by mixing, equipment pressing, curing, cutting and other manufacturing processes. It has good fire resistance (combustion performance can reach Grade A), low thermal conductivity, a good thermal insulation effect, easy construction and a long service life, good security and other advantages, and the GCIB will not reduce its combustion performance and mechanical properties when reducing its density and thermal conductivity [30].

By the end of 2019, China's total urban and rural buildings had reached 62 billion m^2, and building energy consumption accounted for around 22% of the total social energy consumption. Improving building energy efficiency has become one of the most important means to achieve China's carbon peak and neutrality goals in the construction field [31–33]. This paper takes the improved GCIB as the research object. In Section 3, according to the ratios of each material component in the insulation board, the series and parallel theoretical analysis models of the heat conduction theory of the graphite composite insulation board are proposed, and the thermal conductivity limit of the graphite composite insulation board is obtained by using the Fourier heat conduction theory. In Section 4, according to the ratios of each material component, we establish a numerical model of the GCIB with random material distribution. Through numerical simulation, we obtain the average heat flow density distribution relationship of the GCIB, and calculate the thermal conductivity of the GCIB. In Section 5, we configure samples of the GCIB corresponding to the material ratios, and further verify the correctness of the theoretical analysis and numerical simulation through heat conduction tests. This paper studies the thermal conductivity of graphite composite insulation board from three aspects of theoretical analysis, numerical simulation and model tests,; puts forward corresponding theoretical and numerical simulation calculations and analysis methods; verifies the excellent thermal insulation performance of the graphite composite insulation board, and provides a theoretical reference for the promotion and application of graphite composite insulation board.

2. Materials and Methods

2.1. Components of the GCIB

The interior of the GCIB is mainly cemented by aggregates and cementitious materials, mainly consisting of cement, vitrified microspheres, graphite polystyrene particles and silica fume. In order to meet the requirements of thermal conductivity and fire protection in the building code, a DRCD3030 intelligent thermal conductivity tester, electronic balance and other major equipment are used to measure the thermal conductivity according to the lightweight aggregate standard [34] and the guarded hot plate method [35]; the component ratios and thermal conductivity of each material of the improved GCIB are shown in Table 1. Among them, vitrified microspheres and graphite polystyrene particles are the main thermal insulation materials. Cement, as the main cementing material, forms a slurry after adding water to firmly cement the vitrified microspheres and graphite polystyrene particles together. Silica fume, as an additive, can improve the tensile strength, compressive strength, wear resistance, corrosion resistance and flame retardancy of GCIBs, and also reduce the cost of products.

Table 1. The constituents of the GCIB.

Components	Density (kg/m^3)	Mass Percentage (%)	Thermal Conductivity (W/(m · K))
Cement	1135	63.2	0.453
Vitrified microspheres	68	18.1	0.046
Graphite polystyrene particles	16.5	11.6	0.038
Silica fume	338	7.1	0.151

(1) Cement

The test mainly adopts P · O 42.5 ordinary Portland cement [36], with a bulk density of 1200 kg/m^3, a specific surface area of 320 m^2/kg and thermal conductivity of around 0.5 W/(m · K). Its chemical components are shown in Table 2.

Table 2. Chemical components of cement [37].

Components	SiO_2	CaO	Al_2O_3	Fe_2O_3	MgO	SO_3	K_2O	Na_2O	TiO_2	Other Surplus
Proportion (%)	22.9	56.8	7.3	2.7	2.7	2.3	0.6	0.3	0.3	4.1

(2) Vitrified microspheres

A vitrified microsphere is a type of lightweight filler aggregate and thermal insulation material, which has very stable physical and chemical properties, strong anti-aging and weather resistance properties and excellent thermal insulation, fire prevention and sound absorption properties. As a type of green and environmentally friendly building thermal insulation material, the vitrified microsphere has a porous internal structure, a glassy closed external surface and a fully spherical body, with good thermal insulation performance. Compared with the traditional expanded perlite, the vitrified microsphere has weak water absorption capacity and good aging resistance [38].

As one of the main aggregates of the GCIB, the main chemical components are SiO_2, Al_2O_3, CaO. There are different types of vitrified microspheres, which are granular and different in appearance. The size range of vitrified microspheres is 0.1–2 mm, which can be divided into 20–30 mesh, 30–50 mesh, 50–70 mesh, 70–90 mesh and 90–120 mesh according to the size; the appearance of 20–30 mesh vitrified microspheres is as shown in Figure 1. For different sizes of vitrified microspheres, the bulk density is 50–100 kg/m^3, the thermal conductivity is 0.028–0.048 W/m · K, the floating rate is greater than 95%, the vitrification rate of the ball is greater than 95%, the water absorption rate is less than 50% and the melting temperature is 1200 °C. The density of vitrified microspheres is far lower than that of mortar, and the thermal conductivity is significantly lower than that of mortar.

(3) Graphite polystyrene particles

As shown in Figure 2, graphene polyphenylene particles are organic materials with good sphericity, low water absorption, low thermal conductivity (generally less than 0.041 W/(m · K)), excellent thermal insulation performance and a packing density of approximately 1/10 that of the vitrified microsphere [39]. However, they have poor particle grading, a large void ratio, low cementitious strength with cement and poor high-temperature resistance and aging resistance.

Due to the poor grading of graphite polystyrene particles, the double mixed aggregate technology can be used to mix vitrified microspheres and polystyrene particles in an appropriate proportion, which can not only overcome defects such as the high water absorption of the vitrified microsphere and the lower thermal insulation performance of the product in the later period, but also improve the aggregate grading, reduce the cement consumption, meet the dry density requirements and achieve a good thermal insulation effect.

Figure 1. Appearance of vitrified microspheres.

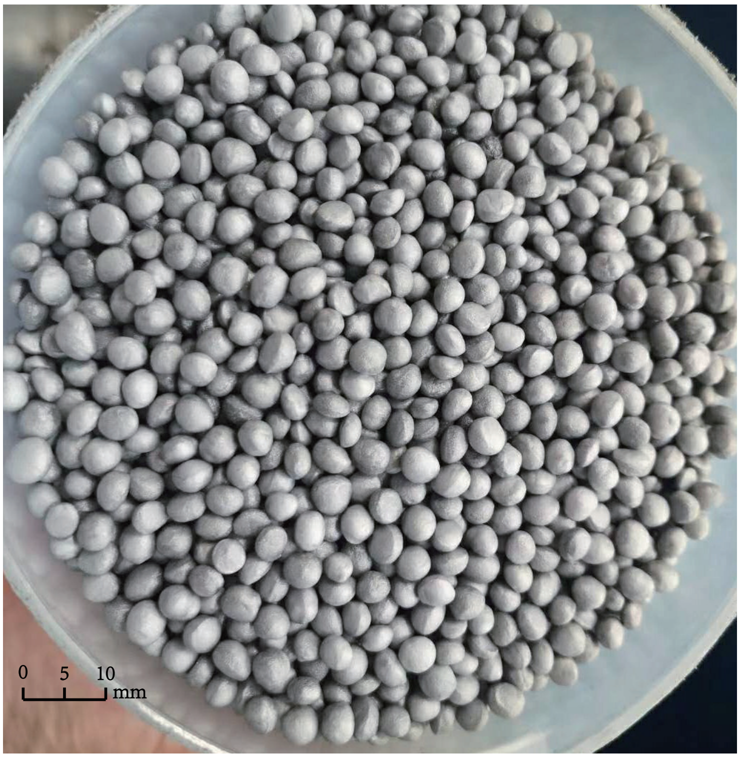

Figure 2. Appearance of graphite polystyrene particles.

(4) Silica fume

In the process of smelting industrial silicon and ferrosilicon in the industrial electric furnace at a high temperature, silica fume (Figure 3) can be obtained through the collection and treatment of waste gas and soot by the capture device [40]. SiO_2 content accounts for around 90% of the total smoke and dust in the escaping smoke and dust, so the main component of silica fume is SiO_2.

Silica fume is not easy to react with other substances, and does not react chemically with most acids and alkalis. Its particles are evenly covered on the surface of the object, with strong corrosion resistance. The particle grading of silica fume is reasonable, which can reduce and eliminate sedimentation and delamination, improve the grading of vitrified microspheres and graphite polystyrene particles and improve the strength, friction resistance, corrosion resistance and other properties of GCIBs.

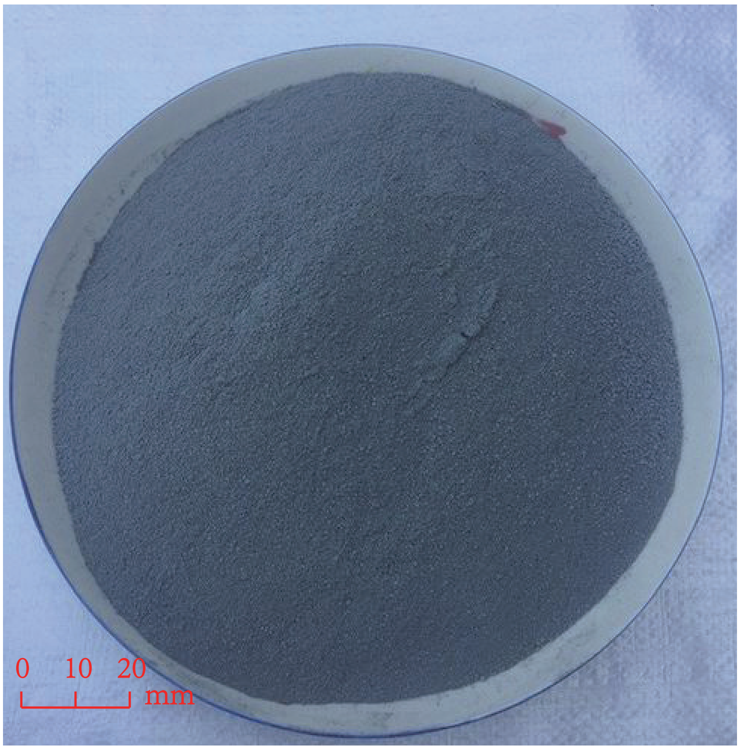

Figure 3. Appearance of silica fume.

2.2. Methods

In this paper, theoretical analysis, numerical simulation and sample tests are used to study the thermal conductivity of GCIBs. Through comparative analysis, the correctness of the test results is verified, and the theoretical and numerical simulation methods that can be used for the thermal conductivity of GCIBs are given. The research technology route is shown in Figure 4.

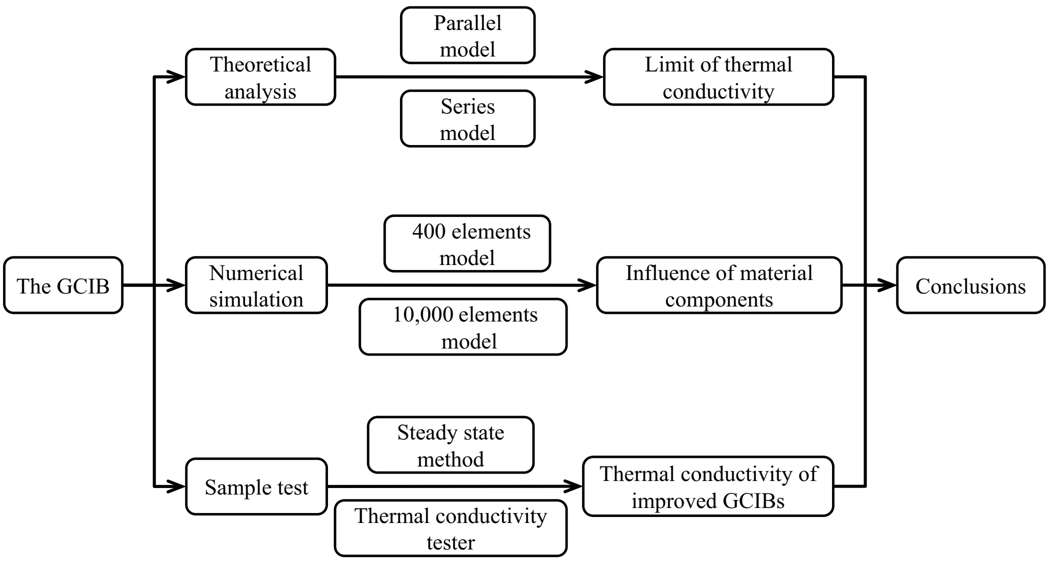

Figure 4. Research technology route.

First, according to the material components of the GCIB, a theoretical analysis model is established. Through series and parallel models, the theoretical calculation expression of the upper and lower limits of the thermal conductivity of the GCIB is obtained. Secondly, the numerical calculation model of the GCIB is established, and the simulation results of the thermal conductivity of the improved GCIB are obtained by using ANSYS for numerical analysis, and the influence law of material components on thermal conductivity is further studied. Next, the sample of the improved GCIB is obtained through the steps of weighing -> mixing -> molding -> curing -> molding. The thermal conductivity of the improved GCIB is measured by the steady-state method. Finally, by comparing the results of the theoretical analysis, numerical simulation and experiment, the final conclusion is drawn.

3. Theoretical Analysis of Heat Conduction in the GCIB

For thermal insulation materials with different material components and structural compositions, the calculation methods of thermal conductivity are different. Song et al. [41] gave a summary of the fundamentals, constituents, constructions and performance of the vacuum insulation panel (VIP). The Simpson [42] model considers the influence of the time effect and obtains the theoretical calculation expression of expanded polystyrene (EPS) foam boards at a given time.

$$\lambda = \lambda_i + \Delta\lambda\left(\left(1 + e^{-L_n(t/c)}\right)^{-1} - 0.5\right) \tag{1}$$

where λ is the thermal conductivity at a given time, the subscript i denotes the initial thermal conductivity and t is the time in days. $\Delta\lambda$ represents the incremental increase in thermal conductivity from the initial value to the final plateau value. C is a time constant that determines the aging rate.

The Wei [43] model studies the thermal conductivity of silica aerogel and proposes a unit cell model for the conductive heat transfer of the xonotlite–aerogel composite insulation material, by simplification; xonotlite-type calcium silicate is considered as a periodical array of hollow cubic structures with connecting bars, and the final heat transfer expression can be written as

$$\begin{aligned} k_c = &\left\{ \frac{(2-\gamma_b)\gamma_a^2\gamma_b}{1-\beta_1\gamma_a} + \frac{\gamma_a^2\left[(1-\gamma_b)^2 - \gamma_c^2\right]}{1-\beta_1\gamma_a\gamma_b} + \frac{2\gamma_a\gamma_c(1-\gamma_a)}{1-\beta_1\gamma_a\gamma_c} \right. \\ &\left. + \frac{\gamma_a^2\gamma_c^2}{1-\beta_1+\beta_1(1-\gamma_b)\gamma_a} + (1-\gamma_a)(1+\gamma_a-2\gamma_a\gamma_c) \right\} \\ &\times \left[\psi k_{\mathrm{ae}} + (1-\psi)k_g\right] \quad (0 < c < a-2h) \end{aligned} \tag{2}$$

$$\begin{aligned} k_c = &\left\{ 1 + \frac{2\gamma_a\gamma_c(1-\gamma_a)}{1-\beta_1\gamma_a\gamma_c} + \frac{(1-\gamma_b)^2\gamma_a^2}{\gamma_a(1-\gamma_b)+(1-\gamma_a+\gamma_a\gamma_b)(1-\beta_1)} \right. \\ &\left. + \frac{(1-\gamma_c^2)\gamma_a^2}{1-\beta_1\gamma_a} + \frac{\gamma_a^2\left[\gamma_c^2 - (1-\gamma_b)^2\right]}{1-\beta_1} + \gamma_a(1-\gamma_a-2\gamma_c+\gamma_a\gamma_c) \right\} \\ &\times \left[\psi k_{\mathrm{ae}} + (1-\psi)k_{\mathrm{g}}\right] \quad (a > c > a-2h) \end{aligned} \tag{3}$$

where $\gamma_a = a/l$, $\gamma_b = 2h/a$ and $\gamma_c = c/a$. a, l, c and h are the structural parameters in the unit cell; $\beta_1 = 1 - k_g/k_{cq}$, k_g and k_{cq} are the effective thermal conductivities of gas in xonotlite-type calcium silicate and the shell of xonotlite-type calcium silicate, respectively. ψ is the filling coefficient of the aerogel, and the expression of k_{ae} is

$$\begin{aligned} k_{\mathrm{ae}} = &\left\{ \frac{\pi a_1^2 a_2^2}{4(1-\beta_2)} + \left(1-a_1^2\right) - \frac{\pi a_1^2(1-a_2^2)}{2\beta_2^2}[\beta_2 + \ln(1-\beta_2)] \right. \\ &\left. + \frac{\pi}{\beta_2}\left(1/\sqrt{1-a_2^2} - a_1\right)\left[\frac{1}{\beta_2 a_1}\ln\frac{1-\beta_2 a_1 a_2}{1-\beta_2 a_1} - (1-a_2)\right] \right\} \times k_{\mathrm{g}} \end{aligned} \tag{4}$$

where $a_1 = d/D$, $a_2 = a/d$. k_g is the gaseous thermal conductivity in the aerogel, which is apparently different from that of the gas in free space. $\beta_2 = 1 - k_g/k_s$, k_g is the gaseous thermal conductivity in the aerogel, and k_s is the solid thermal conductivity in the nanospheres.

Based on Xie et al.'s [44] model and Karamanos et al.'s [45,46] model, Csanády et al. [47] calculated the thermal conductivity factor of the stem in straw-based thermal insulating materials.

$$k_s = [(f_1 + f_2)^2 \times \lambda_{s,g}] \times D \tag{5}$$

where f_1 and f_2 are the stem density of fibers and the material density; $\lambda_{s,g}$ is the the described equation for serial systems and D is the shape-related parameter.

A large number of studies have been conducted on various types of thermal insulation materials. Based on these studies, this section mainly uses series and parallel models to study the thermal conductivity of GCIBs.

In combination with the comprehensive requirements of thermal insulation materials for thermal conductivity and fire resistance, the improved GCIB is composed of four materials. Assuming that the density, mass percentage and thermal conductivity of the various materials constituting the insulation board are known, the volume ratio of each corresponding material of the insulation board is

$$\Omega_i = \frac{\omega_i}{\rho_i} / \sum_{k=1}^{4} \frac{\omega_k}{\rho_k}\,, \quad (i = 1, 2, 3, 4) \tag{6}$$

where Ω_i is the volume ratio of the ith material in the GCIB, ω_i and ω_k are the mass percentages of the ith constituent material, ρ_i is the density of the ith constituent material (unit: $\mathrm{kg/m^3}$), and i is the various materials that make up the GCIB.

The local Fourier heat conduction expression of the four materials constituting the GCIB is [48–50]

$$Q_i = \lambda_i A_i \frac{\Delta T_i}{\Delta d_i}, \quad (i = 1, 2, 3, 4) \tag{7}$$

where Q_i is the heat transferred from the inside and outside of the ith material in the GCIB (unit: W), λ_i is the thermal conductivity of the ith material (unit: $\mathrm{W/(m \cdot K)}$), A_i is the heat transfer area of the ith material (unit: $\mathrm{m^2}$), ΔT_i is the temperature difference between the inside and outside surfaces of the ith material (unit: K), and Δd_i is the thickness of the ith material (unit: m).

The macro Fourier heat conduction expression of the GCIB is [48–50]

$$Q = \lambda A \frac{\Delta T}{\Delta d} \tag{8}$$

where Q is the heat transferred from the inside and outside of the GCIB (unit: W), λ is the equivalent thermal conductivity of the insulation board (unit: $\mathrm{W/(m \cdot K)}$), A is the heat transfer area of the insulation board (unit: $\mathrm{m^2}$), ΔT is the temperature difference between the internal and external surfaces of the insulation board (unit: K), and Δd is the thickness of the insulation board (unit: m).

Since the GCIB is composed of four component materials, in order to obtain the upper and lower limit values of the equivalent thermal conductivity, we assume that the combination of the four materials has two theoretical models, parallel and series, as shown in Figure 5, in which T_h and T_c represent the temperature loads on both sides of the insulation board, respectively.

(1) Upper limit of thermal conductivity in parallel model of insulation board

In the insulation board, the upper bound λ^{ub} of thermal conductivity in the parallel model is the volume average of the constituent materials' thermal conductivity. According to the ratios of each component of the GCIB, the parallel analysis model of the insulation board is established, which meets the basic assumptions.

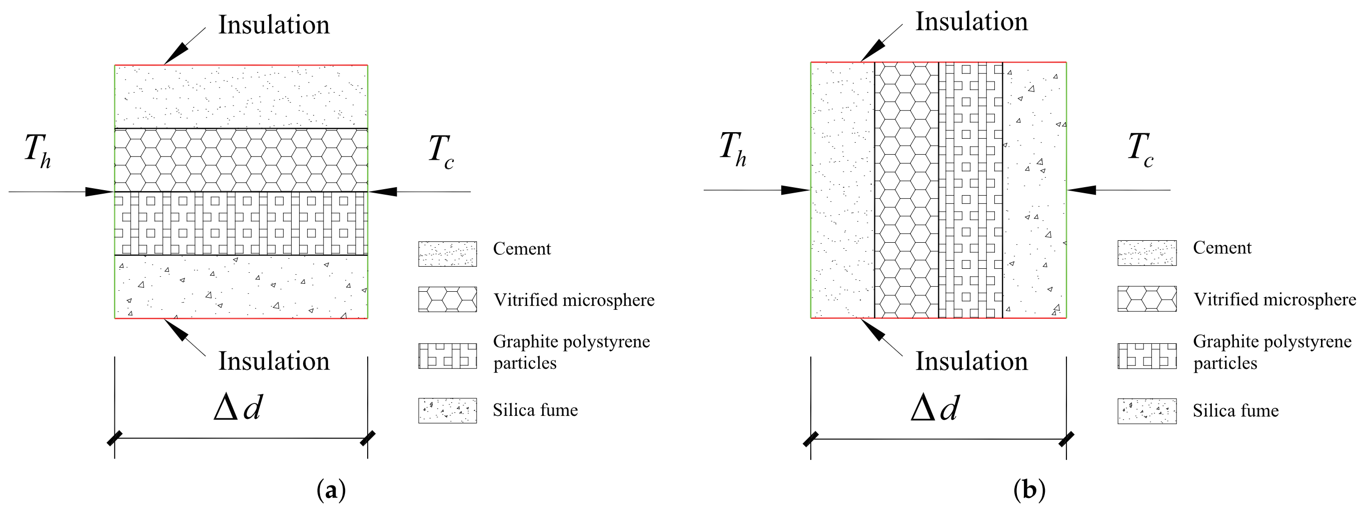

Figure 5. Theoretical model of equivalent thermal conductivity of the GCIB: (**a**) the parallel model; (**b**) the series model.

$$Q = \sum_{k=1}^{4} Q_k, \; A = \sum_{k=1}^{4} A_k \tag{9}$$

$$\Delta T_i = \Delta T, \; \Delta d_i = \Delta d \quad (i = 1, 2, 3, 4) \tag{10}$$

By (9) and (10), we can obtain the volume ratio of various materials in the insulation board:

$$\Omega_i = \frac{A_i \Delta d_i}{A \Delta d} = \frac{A_i}{A} \tag{11}$$

Using the relationship in (10), and combined with (7)–(11), there are

$$\lambda A \frac{\Delta T}{\Delta d} = Q = \sum_{i=1}^{4} Q_i = \sum_{i=1}^{4} \lambda_i A_i \frac{\Delta T}{\Delta d} \tag{12}$$

or

$$\lambda A = \sum_{k=1}^{4} \lambda_k A_k \tag{13}$$

Substituting (11) into (13), we obtain the upper bound equation for calculating the thermal conductivity of the insulation board:

$$\lambda^{\text{ub}} = \sum_{k=1}^{4} \frac{A_k}{A} \lambda_k = \sum_{k=1}^{4} \Omega_k \lambda_k \tag{14}$$

where λ^{ub} is the upper limit value of the thermal conductivity of the GCIB.

(2) Lower limit of thermal conductivity in series model of insulation board

In the insulation board, in order to obtain the lower bound λ^{lb} of the thermal conductivity coefficient in the series model, we first obtain the reciprocal of the constituent materials' thermal conductivity, take the volume average and then calculate the reciprocal. Similarly, the series analysis model of the GCIB is established to meet the basic assumptions

$$Q = Q_i, \; A = A_i, \; (i = 1, 2, 3, 4) \tag{15}$$

$$\Delta T = \sum_{k=1}^{4} \Delta T_i, \; \Delta d = \sum_{k=1}^{4} \Delta d_i \tag{16}$$

By (15) and (16), we can obtain the volume ratio of various components of the insulation board:

$$\Omega_i = \frac{A_i \Delta d_i}{A \Delta d} = \frac{\Delta d_i}{\Delta d} \tag{17}$$

Combining (7), (8) and (15)–(17), we obtain

$$Q = \lambda A \frac{\Delta T}{\Delta d} = \lambda_i A \frac{\Delta T_i}{\Delta d_i} = Q_i \tag{18}$$

By (18), we obtain

$$\lambda \frac{\Delta T}{\Delta d} = \lambda_i \frac{\Delta T_i}{\Delta d_i} \tag{19}$$

i.e.,

$$\frac{\Delta d_i}{\lambda_i \Delta d} \Delta T = \frac{\Delta T_i}{\lambda} \tag{20}$$

By (17) and (20), we obtain

$$\frac{\Omega_i}{\lambda_i} \Delta T = \frac{\Delta T_i}{\lambda} \tag{21}$$

i.e.,

$$\sum_{k=1}^{4} \frac{\Omega_k}{\lambda_k} \Delta T = \sum_{k=1}^{4} \frac{\Delta T_k}{\lambda} \tag{22}$$

Substituting (16) into (22), we obtain the lower bound equation for calculating the thermal conductivity of the GCIB,

$$\sum_{k=1}^{4} \frac{\Omega_k}{\lambda_k} = \frac{1}{\lambda} \tag{23}$$

i.e.,

$$\lambda^{\mathrm{lb}} = 1 / \sum_{k=1}^{4} \frac{\Omega_k}{\lambda_k} \tag{24}$$

where λ^{lb} is the lower limit value of the thermal conductivity in the GCIB (unit: $\mathrm{W/(m \cdot K)}$).

(3) Equivalent thermal conductivity of the GCIB

Assuming that the particles in the GCIB are evenly distributed in all directions, the true value of the equivalent thermal conductivity in the insulation board should be close to the average of its upper and lower limits, hence

$$\lambda^{\mathrm{eq}} = \frac{\lambda^{\mathrm{ub}} + \lambda^{\mathrm{lb}}}{2} = \frac{1}{2 \sum_{k=1}^{4} \frac{\Omega_k}{\lambda_k}} + \frac{1}{2} \sum_{k=1}^{4} \Omega_k \lambda_k \tag{25}$$

4. Numerical Simulation Analysis of Heat Conduction of the GCIB

4.1. Finite Element Model

The GCIB is composed of four materials randomly, and its interior is relatively complex. In order to facilitate numerical simulation, we propose the following assumptions:

- The GCIB is continuous inside, and the material is evenly distributed and dense, without cracks and gaps.
- The four materials inside the insulation board are closely bonded, and the materials are in a binding state during the analysis.
- The thermal conductivity of each constituent material is constant and independent of size and temperature [51].

In order to conduct the numerical simulation on the GCIB, a representative thermal conductivity unit is constructed as shown in Figure 6, and its geometric structure is set as 1 unit [51,52]—that is, the side length of the planar thermal conductivity unit L = 1.

The thermal conductivity of the GCIB is analyzed numerically by using the higher steady state method [51–53]. Planar thermal unit PLANE55 is selected to simulate various materials in the GCIB. The density, mass ratio and thermal conductivity of each component material are shown in Table 1. According to the assumption, since the four component materials are uniformly distributed and dense in the GCIB, the randomly distributed unit numbering program is compiled using Python to establish the calculation and analysis model of the four randomly distributed and dense materials, as shown in Figure 6. According to Figure 6, the finite element model of the GCIB is established by using ANSYS, as shown in Figure 7, which includes the four component materials shown in Table 1, where L = 1 is the size of the heat conduction unit. Since the steady state method is used for numerical simulation, the upper and lower boundary conditions of the finite element model are set to the ideal thermal insulation state, and the left and right ends are, respectively, constant temperature boundaries ($T_h = 50\,\text{K}$ and $T_c = -50\,\text{K}$) along the X axis. We construct different temperature loads on the left and right sides of the finite element model, respectively, and set the upper and lower sides of the Y axis as the insulation boundary state.

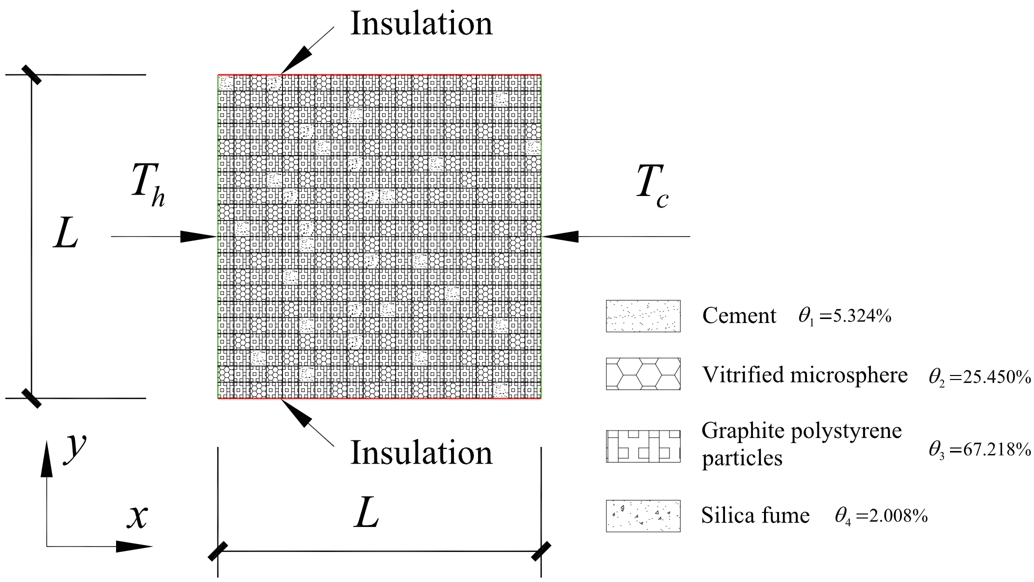

Figure 6. Geometric model of heat conduction unit of the GCIB.

$$T|_{x=0} = T_h \tag{26}$$

$$T|_{x=L} = T_c \tag{27}$$

In the process of steady state heat conduction analysis, the heat exchange caused by convection and radiation (i.e., ideal heat conduction state) is not considered, and the heat conduction in the plane meets

$$\frac{\partial}{\partial x}\left(\lambda\frac{\partial T}{\partial y}\right) + \frac{\partial}{\partial y}\left(\lambda\frac{\partial T}{\partial x}\right) = 0 \tag{28}$$

$$q_x = \lambda\frac{\partial T}{\partial x},\ q_y = \lambda\frac{\partial T}{\partial y} \tag{29}$$

where T is the temperature (unit: K), q is the heat flux vector (unit: W/m^2) and λ is the thermal conductivity (unit: $\text{W/(m} \cdot \text{K)}$).

By (26)–(29), we can obtain the heat flow density distribution and temperature field of the thermal conductivity calculation unit of the GCIB, further calculate the average heat flow density of the thermal conductivity unit and substitute it into Fourier equation (30); thus, we can obtain the thermal conductivity coefficient of the thermal conductivity unit in the insulation board.

$$\lambda = q^{avg} \frac{L}{\Delta T} \tag{30}$$

where λ is the equivalent thermal conductivity of the thermal conductivity calculation unit in the GCIB (unit: $\mathrm{W/(m \cdot K)}$), ΔT is the temperature difference in the direction of heat conduction (i.e., $T_h - T_c$, unit: K) and q^{avg} is the average heat flow density of the thermal conductivity calculation unit of the GCIB (unit: $\mathrm{W/m^2}$).

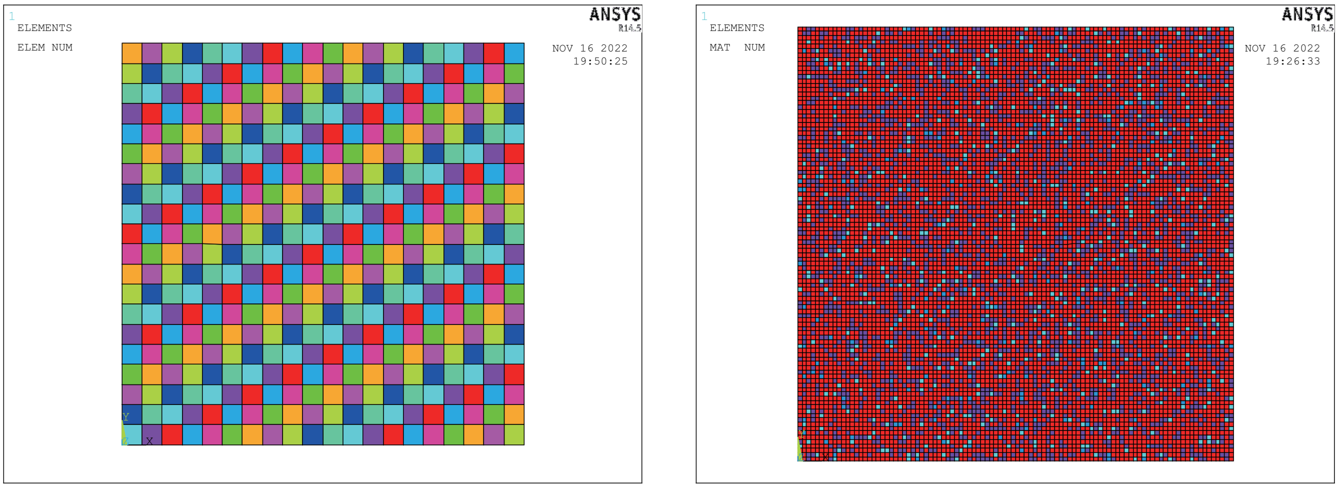

(**a**) (**b**)

Figure 7. Finite element model of heat conduction unit in the GCIB: (**a**) 400 element model; (**b**) 10,000 element model.

4.2. Numerical Simulation Results and Analysis

(1) Thermal conductivity of the improved GCIB

Through the steady state analysis of heat flow, Figure 8 shows the analysis results of the heat flow density of the thermal conductivity calculation unit in the improved GCIB. Through parametric programming, we extract and analyze the average heat flow density of the thermal conductivity calculation unit as $q^{avg400} = 4.603/(\mathrm{W/m^2})$, $q^{avg10{,}000} = 4.593/(\mathrm{W/m^2})$.

According to the calculation results of the average heat flow density obtained from the numerical simulation, using (30), we obtain the thermal conductivity of the two models as $\lambda^{400} \approx \lambda^{10{,}000} = 0.046\ \mathrm{W/(m \cdot K)}$, which is within the range of the theoretical calculation results.

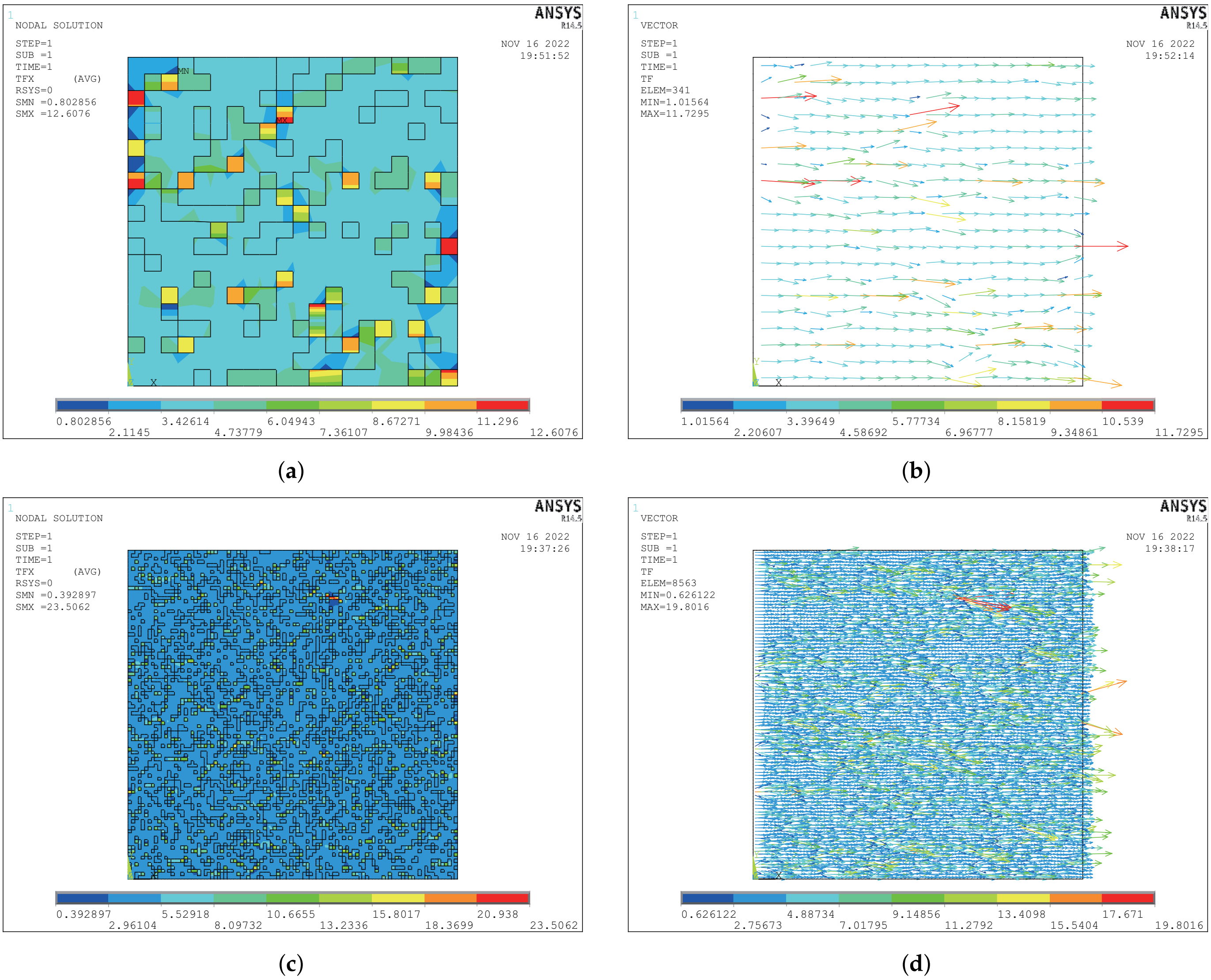

Figure 8. Calculation results of thermal conductivity of the improved GCIB: (**a**) the heat flow density cloud chart (400 units); (**b**) the heat flow density vector chart (400 units); (**c**) the heat flow density cloud chart (10,000 units); (**d**) the heat flow density vector chart (10,000 units).

4.3. Influence of Material Component Ratios

In order to explore the influence of the volume ratio of graphite polystyrene particles on the thermal conductivity in the GCIB, and keep Ω_1 and Ω_2 unchanged (i.e., $\Omega_1 = 5\%$, $\Omega_2 = 25\%$), through numerical simulation, we obtain the influence of the change in the Ω_3 and Ω_4 ratio on the thermal conductivity of the insulation board. Similarly, we keep Ω_2 and Ω_4 unchanged (i.e., $\Omega_2 = 25\%$, $\Omega_4 = 2\%$), and we obtain the effect of the change in the ratios of Ω_3 and Ω_1 on the thermal conductivity of the insulation board. We keep Ω_1 and Ω_4 unchanged (i.e., $\Omega_1 = 5\%$, $\Omega_4 = 2\%$), and we obtain the effect of the change in the ratios of Ω_3 and Ω_2 on the thermal conductivity of the insulation board. Through calculation and analysis, the influence law curve is obtained, as shown in Figure 9.

According to the influence curve shown in Figure 9, we can find that the thermal conductivity of the GCIB decreases rapidly at the initial stage with the increase in the volume ratio of the graphite polystyrene particles. When the volume ratio of the material components approaches 10 (i.e., $\Omega_3/\Omega_4 \rightarrow 10$, $\Omega_3/\Omega_1 \rightarrow 10$, $\Omega_3/\Omega_2 \rightarrow 10$), the thermal conductivity slowly tends to stabilize, and the ratios of material components in the improved GCIB are in a stable range.

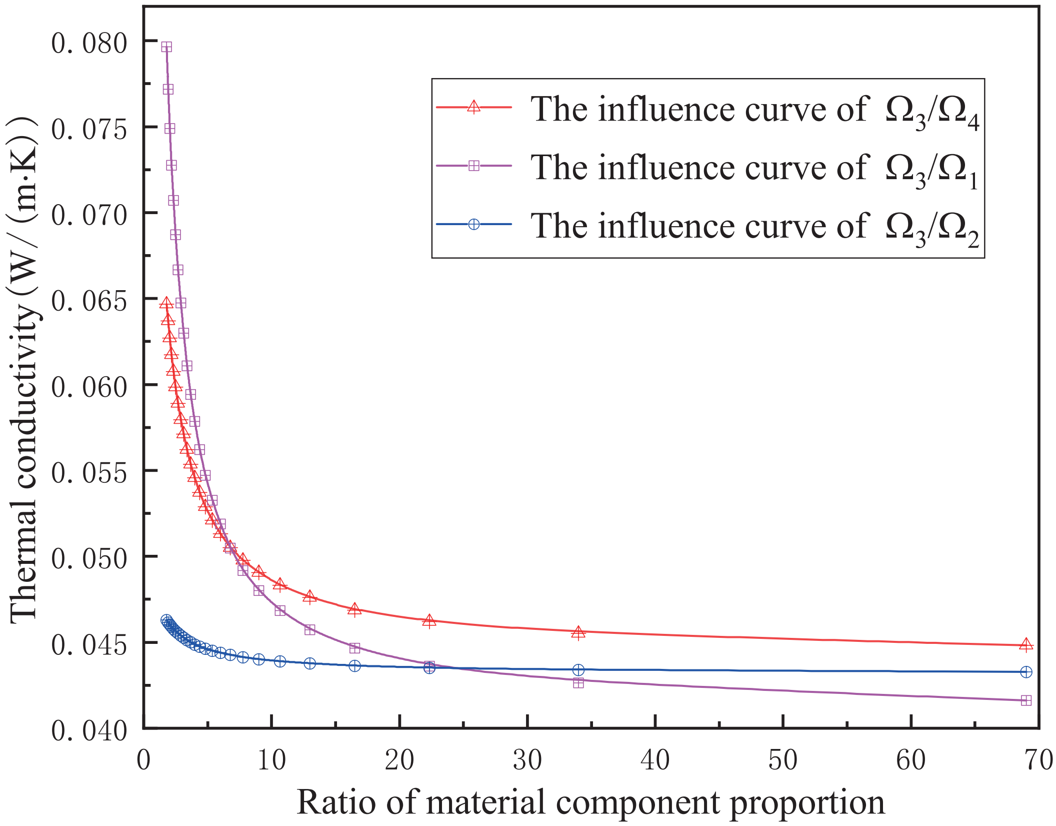

Figure 9. Influence curve of thermal conductivity of the GCIB under different component material ratios.

5. Test Verification of Thermal Conductivity in the GCIB

There are many testing methods for measuring the thermal conductivity of thermal insulation materials [54,55]. The thermal conductivity of thermal insulation materials is affected by various factors (e.g., material types, material components, ambient temperature and humidity) [56], which brings more difficulties to the measurement of the materials' thermal conductivity under actual working conditions. Under laboratory conditions, we use the thermal conductivity meter to build a relatively ideal thermal conductivity environment; the steady state method was used to measure the thermal conductivity of the improved GCIB.

5.1. Measuring Equipment and Principle

The main equipment for measuring the thermal conductivity of the GCIB by the steady state method is the intelligent thermal conductivity tester (device model: DRCD-3030), which is mainly composed of an electric heater, heating disk and radiator, as shown in Figure 10. The measurement range of the thermal conductivity is 0.010–3.000 $W/m \cdot K$, and the test standard adopted is "Thermosetting composite polystyrene foam insulation board" [57].

The temperature of the heating plate is controlled and measured by the temperature control and measurement sensor. The accuracy of the two temperature measurement sensors is 0.1 °C. The upper and lower end surfaces of the GCIB sample are fully contacted with the heating plate and the cooling plate, respectively, similar to a "sandwich"′ structure. During the test, we ignore the horizontal heat transfer, and the heat is only transferred vertically along the upper and lower directions. After the heat transfer, heat dissipation and heat conduction, the system finally reaches a steady state of heat transfer. When the system reaches the steady state, the heating rate, heat transfer rate and heat dissipation rate of the system are all equal. According to the Fourier heat conduction equation, the thermal conductivity can be expressed as [58]

$$\lambda = -mc\left.\frac{\mathrm{d}T}{\mathrm{d}t}\right|_{T=T_2}\frac{(a_P+2h_P)}{(2a_P+2h_P)}\frac{h_B}{(T_1-T_2)}\frac{1}{a_B^2} \quad (31)$$

where T_1 and T_2 are the temperatures of the upper and lower surfaces of the test piece in the steady state; is the mass of the heat sink, is the specific heat capacity of the heat sink ($3.80\times10^2\mathrm{J}\cdot\mathrm{kg}^{-1}\cdot\mathrm{K}^{-1}$), a_P is the side length of the heat sink, h_P is the thickness of the heat sink, a_B is the side length of the sample, h_B is the thickness of the sample, and $\left.\frac{\mathrm{d}T}{\mathrm{d}t}\right|_{T=T_2}$ is the heat dissipation coefficient when the temperature of the heat sink is T_2.

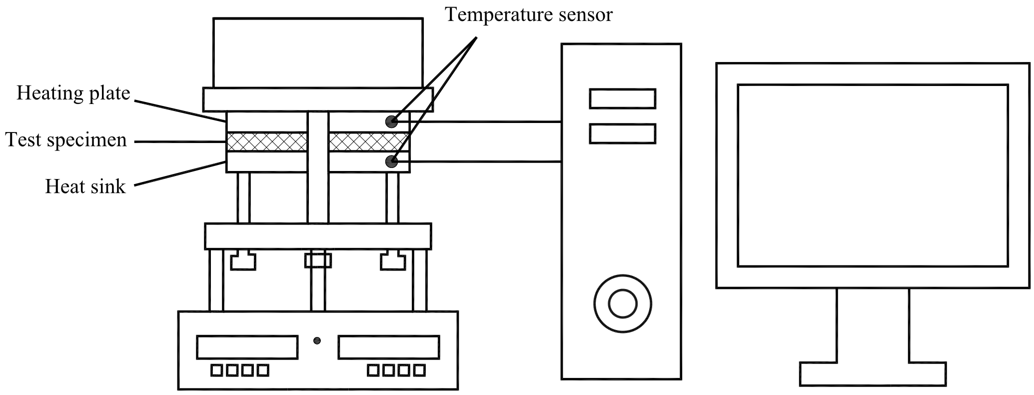

Figure 10. Structure diagram of thermal conductivity tester.

5.2. Test Sample Preparation and Test Process

According to the requirements of the material components shown in Table 1, we weigh the materials in the corresponding ratios, add water to mix them to the flow plastic state and prepare 6 samples with the size of through the setting template, and we ensure that the surface roughness is less than ±2% of the thickness. The preparation process is shown in Figure 11.

We placed the 6 test samples in an electric blast drying oven, slowly raised the temperature to (65 ± 5) °C, dried them to a constant mass (the change rate of the sample mass is 0.2% twice at a constant temperature of 3 h) and then moved them to a dryer to cool them to a normal atmospheric temperature to obtain the test samples, as shown in Figure 12.

We used the thermal conductivity tester to measure the thermal conductivity of the six samples, placed the samples between the heating disk and the cooling disk and used the equipment to start the measurement, as shown in Figure 13. When the cold plate temperature, hot plate temperature and protection temperature are equal to the set temperature, the test reaches a stable state, and the time is counted in seconds after the temperature is stable. If the temperature changes and becomes stable again, the time will be counted again. When the power is stable, the thermal conductivity is also stable (three decimal places are stable, and the thermal conductivity of the insulation board can be determined when the stability time is 10,000 s or more).

(**a**) (**b**)

Figure 11. Preparation of the GCIB samples: (**a**) mixing mixture; (**b**) mixture molding.

Figure 12. Samples of the prepared GCIB.

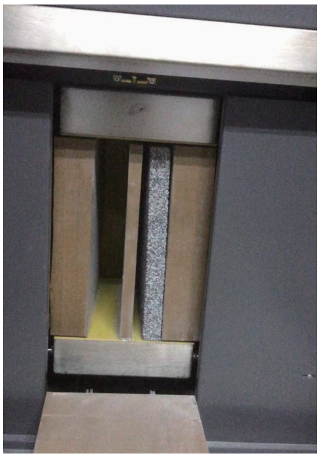

Figure 13. Thermal conductivity test of the GCIB.

5.3. Test Result

Through the tests on 6 groups of samples, we obtained the process change curve of the thermal conductivity in the GCIB, as shown in Figure 14. When the thermal conductivity test reached a steady state, the temperature of the cold zone was kept at 15 °C and the temperature of the hot zone was kept at 35 °C.

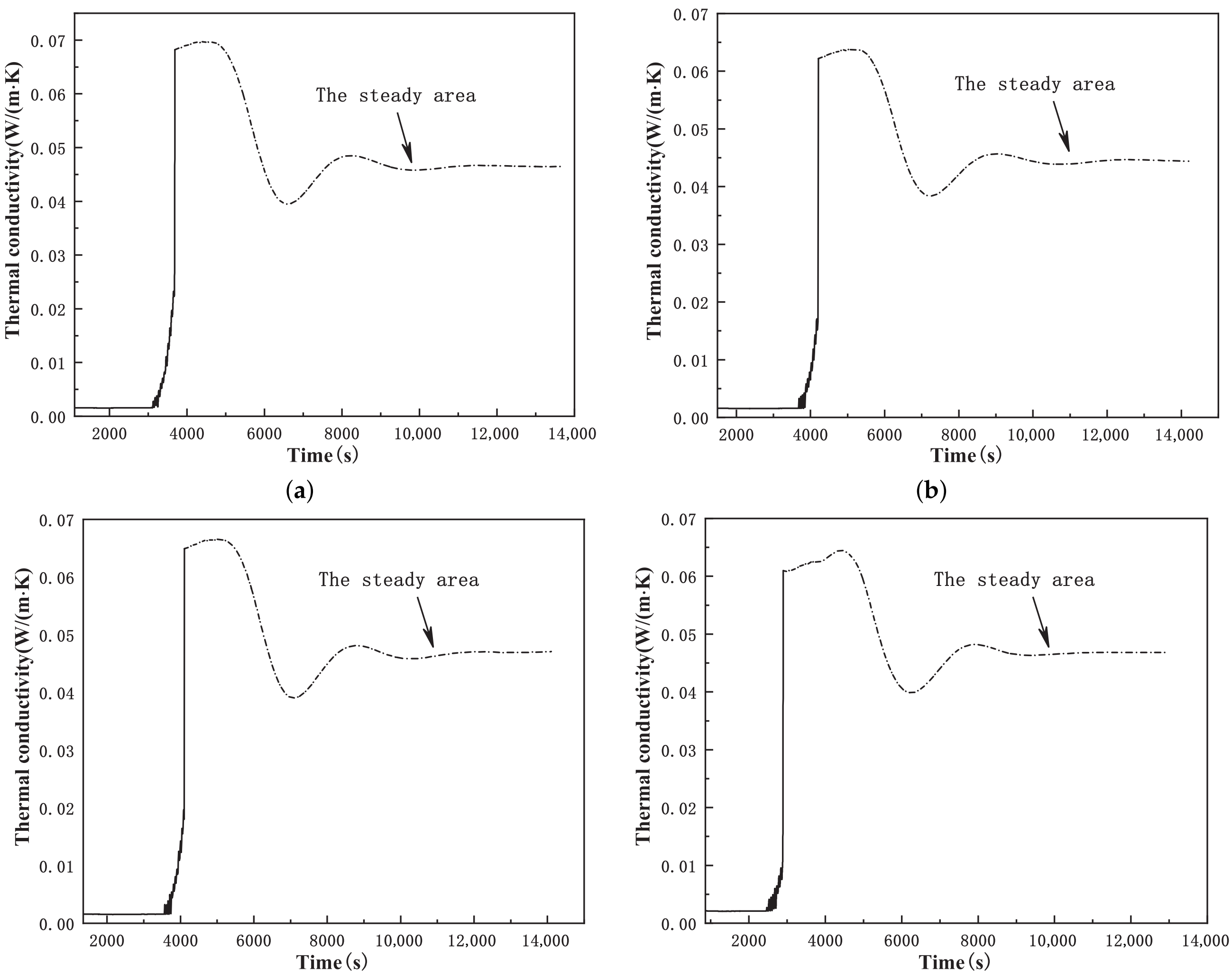

(a) (b) (c) (d)

Figure 14. *Cont.*

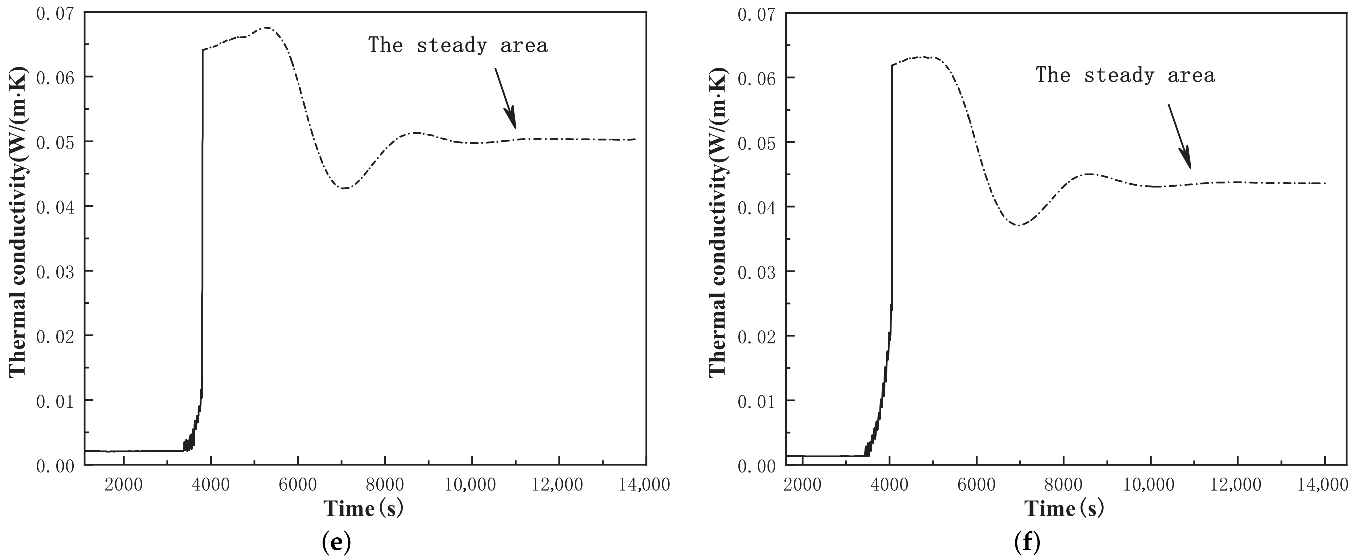

Figure 14. Test curve of thermal conductivity in the GCIB: (**a**) 1# insulation board; (**b**) 2# insulation board; (**c**) 3# insulation board; (**d**) 4# insulation board; (**e**) 5# insulation board; (**f**) 6# insulation board.

The test results show that the temperature of the insulation board basically enters the equilibrium and stable stage in the cold and hot areas in around 4000 s, and the system reaches the stable state in around 12,000 s. We take the average of the thermal conductivity test results of 3000 s in the last stage as the final thermal conductivity of the insulation board, and the test results are shown in Table 3. According to the test results in Table 3, the thermal conductivity of the GCIB is within the range of 0.044–0.050 $W/(m \cdot K)$. The test results of $1\# - 6\#$ insulation boards were taken as the analysis object. The average thermal conductivity of the thermal insulation board is $\lambda^s = 0.047$ $W/(m \cdot K)$, and the standard deviation is $\sigma^s = 0.002$ $W/(m \cdot K)$.

Table 3. Thermal conductivity of the test sample.

Insulation Board No.	1#	2#	3#	4#	5#	6#	Average	Standard Deviation
Thermal conductivity (W/(m·K))	0.047	0.044	0.047	0.047	0.050	0.044	0.047	0.002

6. Results and Discussion

6.1. Comparison of Calculation Results of the GCIB

(1) Theoretical calculation result

Substituting the data of the improved GCIB in Table 1 into (6), we can obtain the volume ratio of each component material:

$$\begin{aligned}
\Omega_1 &= \frac{\omega_1}{\rho_1} / \sum_{k=1}^{4} \frac{\omega_k}{\rho_k} = 5.324\%, \quad \Omega_2 = \frac{\omega_2}{\rho_2} / \sum_{k=1}^{4} \frac{\omega_k}{\rho_k} = 25.450\% \\
\Omega_3 &= \frac{\omega_3}{\rho_3} / \sum_{k=1}^{4} \frac{\omega_k}{\rho_k} = 67.218\%, \quad \Omega_4 = \frac{\omega_4}{\rho_4} / \sum_{k=1}^{4} \frac{\omega_k}{\rho_k} = 2.008\%
\end{aligned} \tag{32}$$

According to the thermal conductivity of each material in Table 1, substituting the volume ratio in (32) into (14), we can obtain the upper limit value of the thermal conductivity in the parallel model of the improved GCIB:

$$\lambda^{\text{ub}} = \sum_{k=1}^{4} \Omega_k \lambda_k = 0.064 \ (W/(m \cdot K)) \tag{33}$$

By (22), we can obtain the lower limit value of the thermal conductivity in the series model of the improved GCIB:

$$\lambda^{\text{lb}} = 1/\sum_{k=1}^{4} \frac{\Omega_k}{\lambda_k} = 0.042\ (\text{W}/(\text{m} \cdot \text{K})) \tag{34}$$

Assuming that the constituent particles of the improved GCIB are uniformly distributed in all directions, and the true value of the thermal conductivity in the insulation board is between λ^{lb} and λ^{ub}, we can approximately take the equivalent thermal conductivity as the average of the upper and lower limit values:

$$\lambda^{\text{eq}} = \frac{\lambda^{\text{ub}} + \lambda^{\text{lb}}}{2} = 0.053\ (\text{W}/(\text{m} \cdot \text{K})) \tag{35}$$

(2) Comparison of results

Through the analysis of series and parallel theoretical models, the maximum thermal conductivity of the improved GCIB is $\lambda^{\text{ub}} = 0.064\,\text{W}/(\text{m} \cdot \text{K})$, the minimum value is $\lambda^{\text{lb}} = 0.042\,\text{W}/(\text{m} \cdot \text{K})$, and the equivalent value is $\lambda = 0.053\,\text{W}/(\text{m} \cdot \text{K})$. According to Section 4.2, the calculation results of the thermal conductivity of the two numerical models are $\lambda^{400} \approx \lambda^{10,000} = 0.046\,\text{W}/(\text{m} \cdot \text{K})$. Through the sample test, we obtain the average thermal conductivity of the improved GCIB as $\lambda^{\text{s}} = 0.047\,\text{W}/(\text{m} \cdot \text{K})$.

Through the comparison of the theoretical analysis, numerical simulation and test results, we found that the sample test results are in good agreement with the numerical simulation analysis results, and the error of the two results is within 0.5%, which is closer to the calculation results of the series theoretical model, between λ^{ub} and λ^{eq}.

6.2. Comparison of the Influence of Material Component Ratios

According to (14), (24) and (25), the theoretical thermal conductivity of GCIBs under different material ratios can be obtained. Then, according to Sections 4.3 and 5.3, the theoretical results, numerical simulation results and experimental results are compared, as shown in Figure 15.

According to Figure 15, it is found that the thermal conductivity of the GCIB decreases in two stages as the proportion of graphite polystyrene particles increases. In the first stage, $\Omega_3/\Omega_4 \leq 10$ ($\Omega_3/\Omega_1 \leq 10$ or $\Omega_3/\Omega_2 \leq 10$); as the Ω_3/Ω_4 (Ω_3/Ω_1 or Ω_3/Ω_2) ratio increases, the thermal conductivity decreases obviously. In the second stage, $\Omega_3/\Omega_4 > 10$ ($\Omega_3/\Omega_1 > 10$ or $\Omega_3/\Omega_2 > 10$); as the Ω_3/Ω_4 (Ω_3/Ω_1 or Ω_3/Ω_2) ratio increases, the thermal conductivity decreases slowly. The results of the numerical simulation and sample test have strong agreement, and the analysis results of the numerical simulation are closer to the lower limit value of the theoretical results. The change curve of the numerical simulation of thermal conductivity is between the theoretical lower limit value curve and the equivalent value curve.

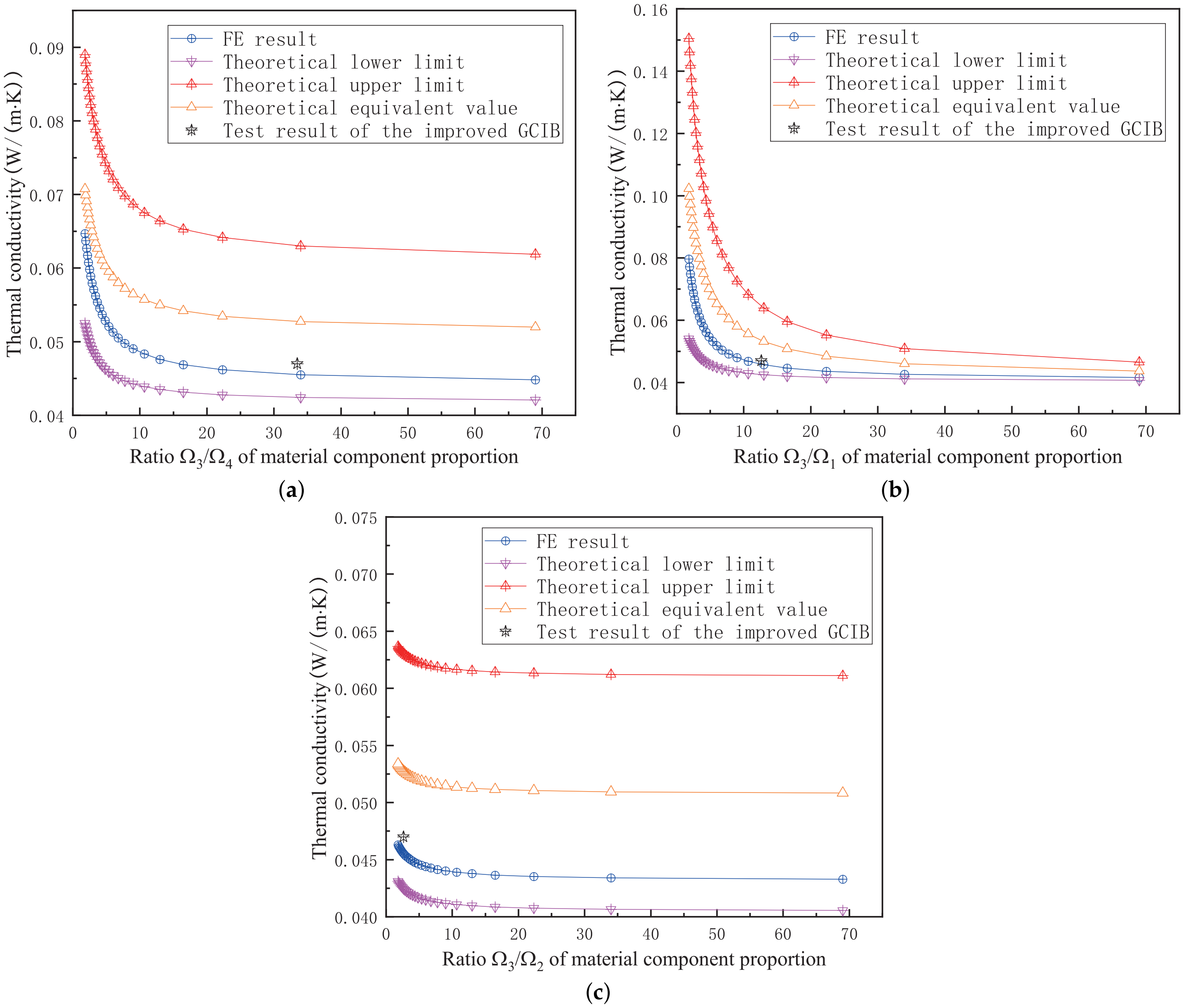

Figure 15. Influence curve of thermal conductivity under component material proportion ratio Φ: **(a)** $\Phi = \Omega_3/\Omega_4$; **(b)** $\Phi = \Omega_3/\Omega_1$; **(c)** $\Phi = \Omega_3/\Omega_2$.

7. Conclusions

Through theoretical analysis, numerical simulation and experimental tests on the improved GCIB, several conclusions are derived as follows.

1. The series and parallel models of the GCIB were proposed, which were used to calculate the thermal conductivity of the improved GCIB. The theoretical range of the thermal conductivity of the improved GCIB was obtained.
2. According to the ratios of each material component in the improved composite insulation board, we established a numerical analysis model of the insulation board with a random distribution of each material component. Through analysis, we obtained the average heat flow density of the thermal conductivity calculation unit. According to the Fourier heat conduction calculation formula, we further obtained the thermal conductivity of the insulation board, which was within the reasonable range of theoretical calculation.
3. Through numerical simulation, we studied the influence of the volume fraction of graphite polystyrene particles on the thermal conductivity of the GCIB. With the increase in the volume ratio of graphite polystyrene particles, the thermal conductivity of the GCIB decreased rapidly at the initial stage. When the volume ratio approached

10 (i.e., $\Omega_3/\Omega_4 \rightarrow 10$, $\Omega_3/\Omega_1 \rightarrow 10$, $\Omega_3/\Omega_2 \rightarrow 10$), the thermal conductivity value tended to be stable.

4. The thermal conductivity of the improved GCIB was obtained through the testing of the samples. The test results were within the range of the theoretical calculation results, and the numerical simulation results were in good agreement with the error within 0.5%.

In this paper, the theoretical calculation model of the GCIB was first given. Through numerical simulation and test research, we verified the thermal conductivity of the improved GCIB. The research results have high theoretical and application value. The ratios of each component material in the improved GCIB are within a reasonable range (i.e., $\Omega_3/\Omega_4 \rightarrow 10$, $\Omega_3/\Omega_1 \rightarrow 10$, $\Omega_3/\Omega_2 \rightarrow 10$); however, there is still considerable space for optimization and improvement. We hope to achieve better improvements in future research.

Author Contributions: Conceptualization, G.L.; Software, Z.J.; Formal analysis, G.L. and T.Z.; Investigation, G.L. and M.H.; Resources, G.L.; Data curation, T.Z. and M.H.; Writing—original draft preparation, T.Z. and G.L.; Writing—review and editing, T.Z. and Y.G.; Project administration, T.Z. All authors have read and agreed to the published version of the manuscript.

Funding: This research was supported by the Jiangxi Provincial Natural Science Foundation (Award No. 20224BAB214072) and the Jiangxi Province Education Science "14th Five-Year Plan" Project (Award No. 22QN007).

Data Availability Statement: The data of this study are available from the corresponding author upon request.

Conflicts of Interest: The authors declare no conflict of interest.

References

1. Pásztory, Z. An overview of factors influencing thermal conductivity of building insulation materials. *J. Build. Eng.* **2021**, *44*, 102604.
2. Capuano, L. *International Energy Outlook 2018 (IEO2018)*; US Energy Information Administration (EIA): Washington, DC, USA, 2018; p. 21.
3. Domínguez-Muñoz, F.; Anderson, B.; Cejudo-López, J.M.; Carrillo-Andrés, A. Uncertainty in the thermal conductivity of insulation materials. *Energy Build.* **2010**, *42*, 2159–2168. [CrossRef]
4. Chapter 31: Energy Estimating and Modeling Methods. In *ASHRAE Handbook*; American Society of Heating, Refrigerating, and Air-Conditioning Engineers: Atlanta, GA, USA, 2001.
5. Peavy, B.A. A heat transfer note on temperature dependent thermal conductivity. *J. Therm. Insul. Build. Envel.* **1996**, *20*, 76–90. [CrossRef]
6. Schiavoni, S.; Bianchi, F.; Asdrubali, F. Insulation materials for the building sector: A review and comparative analysis. *Renew. Sustain. Energy Rev.* **2016**, *62*, 988–1011. [CrossRef]
7. Abu-Jdayil, B.; Mourad, A.H.; Hittini, W.; Hassan, M.; Hameedi, S. Traditional, state-of-the-art and renewable thermal building insulation materials: An overview. *Constr. Build. Mater.* **2019**, *214*, 709–735. [CrossRef]
8. Yüksel, N. The review of some commonly used methods and techniques to measure the thermal conductivity of insulation materials. In *Insulation Materials in Context of Sustainability*; IntechOpen: London, UK , 2016.
9. Lakatos, Á.; Kovács, Z. Comparison of thermal insulation performance of vacuum insulation panels with EPS protection layers measured with different methods. *Energy Build.* **2021**, *236*, 110771. [CrossRef]
10. Berardi, U. The impact of aging and environmental conditions on the effective thermal conductivity of several foam materials. *Energy* **2019**, *182*, 777–794. [CrossRef]
11. Kumar, D.; Alam, M.; Zou, P.X.; Sanjayan, J.G.; Memon, R.A. Comparative analysis of building insulation material properties and performance. *Renew. Sustain. Energy Rev.* **2020**, *131*, 110038. [CrossRef]
12. Yang, J.; Wu, H.; Xu, X.; Huang, G.; Xu, T.; Guo, S.; Liang, Y. Numerical and experimental study on the thermal performance of aerogel insulating panels for building energy efficiency. *Renew. Energy* **2019**, *138*, 445–457. [CrossRef]
13. König, J.; Nemanič, V.; Žumer, M.; Petersen, R.R.; Østergaard, M.B.; Yue, Y.; Suvorov, D. Evaluation of the contributions to the effective thermal conductivity of an open-porous-type foamed glass. *Constr. Build. Mater.* **2019**, *214*, 337–343. [CrossRef]
14. Lamy-Mendes, A.; Pontinha, A.D.R.; Alves, P.; Santos, P.; Durães, L. Progress in silica aerogel-containing materials for buildings' thermal insulation. *Constr. Build. Mater.* **2021**, *286*, 122815. [CrossRef]
15. Li, X.; Peng, C.; Liu, L. Experimental study of the thermal performance of a building wall with vacuum insulation panels and extruded polystyrene foams. *Appl. Therm. Eng.* **2020**, *80*, 115801. [CrossRef]

16. Wang, Y.; Zhang, S.; Wang, D.; Liu, Y. Experimental study on the influence of temperature and humidity on the thermal conductivity of building insulation materials. *Energy Built Environ.* 2022, *in press*. [CrossRef]
17. Pfundstein, M.; Gellert, R.; Spitzner, M.; Rudolphi, A. *Insulating Materials: Principles, Materials, Applications*; Walter de Gruyter: Berlin, Germany, 2012.
18. Zhang, H. *Building Materials in Civil Engineering*; Elsevier: Amsterdam, The Netherlands, 2011.
19. Omer, S.A.; Riffat, S.B.; Qiu, G. Thermal insulations for hot water cylinders: A review and a conceptual evaluation. *Build. Serv. Eng. Res. Technol.* **2007**, *28*, 275–293. [CrossRef]
20. Petrosyan, A.L. The Influence of the Properties of Thermal-Insulation Materials on the Thermomoist Indicators of a Building. *Key Eng. Mater.* **2022**, *906*, 125–133. [CrossRef]
21. Khoukhi, M. The combined effect of heat and moisture transfer dependent thermal conductivity of polystyrene insulation material: Impact on building energy performance. *Energy Build.* **2018**, *169*, 228–235. [CrossRef]
22. Berardi, U.; Nosrati, R.H. Long-term thermal conductivity of aerogel-enhanced insulating materials under different laboratory aging conditions. *Energy* **2018**, *147*, 1188–1202. [CrossRef]
23. Berardi, U.; Tronchin, L.; Manfren, M.; Nastasi, B. On the effects of variation of thermal conductivity in buildings in the Italian construction sector. *Energies* **2018**, *11*, 872. [CrossRef]
24. Al-Homoud, M.S. Performance characteristics and practical applications of common building thermal insulation materials. *Build. Environ.* **2005**, *40*, 353–366. [CrossRef]
25. Berardi, U.; Naldi, M. The impact of the temperature dependent thermal conductivity of insulating materials on the effective building envelope performance. *Energy Build.* **2017**, *144*, 262–275. [CrossRef]
26. Wu, J.W.; Sung, W.F.; Chu, H.S. Thermal conductivity of polyurethane foams. *Int. J. Heat Mass Transf.* **1999**, *42*, 2211–2217. [CrossRef]
27. Hoseini, A.; McCague, C.; Andisheh-Tadbir, M.; Bahrami, M. Aerogel blankets: From mathematical modeling to material characterization and experimental analysis. *Int. J. Heat Mass Transf.* **2016**, *93*, 1124–1131. [CrossRef]
28. Majumder, A.; Canale, L.; Mastino, C.C.; Pacitto, A.; Frattolillo, A.; Dell'Isola, M. Thermal characterization of recycled materials for building insulation. *Energies* **2021**, *14*, 3564. [CrossRef]
29. Hossain, M.D.; Hassan, M.K.; Akl, M.; Pathirana, S.; Rahnamayiezekavat, P.; Douglas, G.; Bhat, T.; Saha, S. Fire Behaviour of Insulation Panels Commonly Used in High-Rise Buildings. *Fire* **2022**, *5*, 81. [CrossRef]
30. Zhang, J.; Cao, Y.; Wang, X. Study on Properties of Graphite Polystyrene Permeable Composite Insulation Board. *IOP Conf. Ser. Mater. Sci. Eng.* **2020**, *744*, 012043. [CrossRef]
31. Li, B.; Huo, Y.; Yin, S. Sustainable financing efficiency and environmental value in China's energy conservation and environmental protection industry under the double carbon target. *Sustainability* **2022**, *14*, 9604. [CrossRef]
32. Huang, X.; Lu, X.; Sun, Y.; Yao, J.; Zhu, W. A Comprehensive Performance Evaluation of Chinese Energy Supply Chain under "Double-Carbon" Goals Based on AHP and Three-Stage DEA. *Sustainability* **2022**, *14*, 10149. [CrossRef]
33. Moayedi, H.; Mosavi, A. Double-target based neural networks in predicting energy consumption in residential buildings. *Energies* **2021**, *14*, 1331. [CrossRef]
34. *GB/T 17431.2-2010*; Lightweight Aggregates and Its Test Methods—Part 2: Test Methods for Lightweight Aggregates. Standardization Administration of China: Beijing, China, 2010.
35. *ISO8302:1991*; Thermal Insulation—Determination of Steady-State Thermal Resistance and Related Properties—Guarded Hot Plate Apparatus. ISO: Geneva, Switzerland, 1991.
36. Bentz, D.P. A review of early-age properties of cement-based materials. *Cem. Concr. Res.* **2008**, *38*, 196–204. [CrossRef]
37. Zhou, C. *Research on the Preparation and Engineering Properties of High Performance Glass Hollow Bead Thermal Insulation Mortar*; East China University of Technology: Fuzhou, China, 2022.
38. Gong, J.; Duan, Z.; Sun, K.; Xiao, M. Waterproof properties of thermal insulation mortar containing vitrified microsphere. *Constr. Build. Mater.* **2016**, *123*, 274–280. [CrossRef]
39. Lakatos, Á.; Deák, I.; Berardi, U. Thermal characterization of different graphite polystyrene. *Int. Rev. Appl. Sci. Eng.* **2018**, *9*, 163–168. [CrossRef]
40. Khan, M.I.; Siddique, R. Utilization of silica fume in concrete: Review of durability properties. *Resour. Conserv. Recycl.* **2011**, *57*, 30–35. [CrossRef]
41. Song, K.; Mukhopadhyaya, P. Vacuum insulation panels (VIPS) in building envelope constructions: An overview. *Int. Rev. Appl. Sci. Eng.* **2016**, *7*, 113–119. [CrossRef]
42. Simpson, A.; Rattigan, I.G.; Kalavsky, E.; Parr, G. Thermal conductivity and conditioning of grey expanded polystyrene foams. *Cell. Polym.* **2020**, *39*, 238–262. [CrossRef]
43. Wei, G.; Liu, Y.; Zhang, X.; Yu, F.; Du, X. Thermal conductivities study on silica aerogel and its composite insulation materials. *Int. J. Heat Mass Transf.* **2011**, *54*, 2355–2366. [CrossRef]
44. Xie, T.; He, Y.L.; Li, Y.S.; Tao, W.Q. Theoretical and Numerical Study on Thermal Properties of Fibrous Insulation Materials. In Proceedings of the 14th Minsk International Forum on Heat and Mass Transfer, Minsk, Belarus, 10–13 September 2012.
45. Karamanos, A.; Papadopoulos, A.M.; Anastasellos, D. Heat transfer phenomena in fibrous insulating materials. In Proceedings of the 2004 WSEAS/IASME International Conference on Heat and Mass, Corfu, Greece, 16–19 August 2004.

46. Karamanos, A.; Hadiarakou, S.; Papadopoulos, A.M. The impact of temperature and moisture on the thermal performance of stone wool. *Energy Build.* **2008**, *40*, 1402–1411. [CrossRef]
47. Csanády, D.; Fenyvesi, O.; Nagy, B. Heat transfer in straw-based thermal insulating materials. *Materials* **2021**, *14*, 4408. [CrossRef] [PubMed]
48. Narasimhan, T.N. Fourier's heat conduction equation: History, influence, and connections. *Rev. Geophys.* **1999**, *37*, 151–172. [CrossRef]
49. Greiner, W.; Neise, L.; Stöcker, H. *Thermodynamics and Statistical Mechanics*; Springer Science & Business Media: Berlin/Heidelberg, Germany, 2012.
50. Stowe, K. *An Introduction to Thermodynamics and Statistical Mechanics*; Cambridge University Press: Cambridge, UK, 2007.
51. Zhang, Y.F.; Zhao, Y.H.; Bai, S.L.; Yuan, X. Numerical simulation of thermal conductivity of graphene filled polymer composites. *Compos. Part B Eng.* **2016**, *106*, 324–331. [CrossRef]
52. Liu, H.; Tian, Y.; Jiao, J.; Wu, X.; Li, Z. Thermal conductivity modeling of hollow fiber-based porous structures for thermal insulation applications. *J. -Non-Cryst. Solids* **2022**, *575*, 121188. [CrossRef]
53. Hiroshi, H.; Minoru, T. Equivalent inclusion method for steady state heat conduction in composites. *Int. J. Eng. Sci.*. **1986**, *24*, 1159–1172. [CrossRef]
54. Sanchez-Calderon, I.; Merillas, B.; Bernardo, V.; Rodríguez-Pérez, M.Á. Methodology for measuring the thermal conductivity of insulating samples with small dimensions by heat flow meter technique. *J. Therm. Anal. Calorim.* **2022**, *147*, 12523–12533. [CrossRef]
55. Baldinelli, G.; Bianchi, F.; Gendelis, S.; Jakovics, A.; Morini, G.L.; Falcioni, S.; Fantucci, S.; Serra, V.; Navacerrada, M.; Díaz, C.; et al. Thermal conductivity measurement of insulating innovative building materials by hot plate and heat flow meter devices: A Round Robin Test. *Int. J. Therm. Sci.* **2019**, *139*, 25–35. [CrossRef]
56. Wang, Y.; Liu, K.; Liu, Y.; Wang, D.; Liu, J. The impact of temperature and relative humidity dependent thermal conductivity of insulation materials on heat transfer through the building envelope. *J. Build. Eng.* **2022**, *46*, 103700. [CrossRef]
57. *JG/T 536-2017*; Thermosetting Composite Polystyrene Foam Insulation Board. Ministry of Housing and Urban-Rural Development of the People's Republic of China: Beijing, China, 2017.
58. Xie, Y.; Dang, Y.; Wang, Z. *College Physics Experiment*; Higher Education Press: Beijing, China, 2017.